

Full Length Article

Pressurization, intercalation, doping, and elements: An empirical study of superconductivity near perturbation onsets



Shermane M. Benjamin

The National High Magnetic Field Laboratory, 1800 E. Paul Dirac Drive, Tallahassee, FL 32310, USA

ARTICLE INFO

Keywords:
 Superconductivity
 Ideal gas law
 Empirical
 Doping
 Intercalation
 Critical pressure
 Phenomenological theory
 Predicting T_c

ABSTRACT

Superconductivity is a phenomenon arising from cooperative electron behavior. However, correlations among (1) the minimum tuning parameter required for emergence, (2) the superconducting transition temperature resulting from minimal tuning, and (3) the host's physical/chemical properties still elude the scientific community. Recent empirical investigations, such as those revealing ideal gas-like correlations at the onset of superconductivity in intercalated superconductors, motivate this study. Our investigation reports similar findings in systems (>170 compounds) exhibiting superconductivity through other perturbative means, such as single-element doping. In general, statistical measures, including distance correlation analyses (\neq linear regression fit) of thermodynamic variables, indicate the presence of empirical relationships near the superconducting onset of systematically tuned compounds. These relations involve unit cell volume (V), the number of valence electrons (N), and the superconducting transition temperature (T_c). Note: The author's primary aim is not to validate or challenge BCS theory; it is instead to focus on leveraging methodology led by available data to enhance the exploration and development of innovative and cost-effective superconductors.

1. Introduction

There are various pathways to superconductivity. These include unconventional routes such as gating [1–3], stacking [4], and twisting [5], and long-established techniques like intercalation [6–8], doping [9–11], and pressurization [12–14]. All methods reliably transform nonsuperconducting materials into superconductors. Pressurization has even successfully produced compounds with predicted signatures of high-temperature superconductivity [15–17].

A common characteristic of these established pathways is the generic dome-like phase diagram depicted in Fig. 1. Thus far, this hallmark feature has not been systematically linked to the chemistry or structure of superconductors. These diagrams typically illustrate superconductivity (i.e., measurable T_c) appearing within specific chemical (e.g., dopant concentration) or physical (e.g., hydrostatic pressure) control parameter values. Some also display monotonic suppression of magnetic order and/or structural transitions preceding the emergence of superconductivity [18,19], while others allow the coexistence of these states [20,21].

The often-serendipitous appearance of the superconducting region has long perplexed the materials science community. However, recent studies [22–23] revealed the chemical boundary between the normal and superconducting state, as illustrated in Fig. 1, empirically follows

Eq. (1) for intercalated superconductors. Notably, available data suggests the rule is independent of the possible emergence and coexistence of other quantum states (e.g., magnetism) with similar energy.

$$P_{int-o}V = x_o N \kappa T_{c-o} \quad (1)$$

The variables P , V , x_o , N , κ , and T_{c-o} are the calculated intercalant pressure ($:= P_{int-o} \approx 1$ atm), unit cell volume, intercalant atomic concentration at the onset of superconductivity, number of intercalant valence electrons ($:= N_{int}$; s and d electrons for all transition elements), Boltzmann constant, and critical temperature at the onset concentration, respectively. Since the investigated compounds have similar P , essentially, Eq. (1) implies that the calculated electron perturbation density ($\rho_{int-o} = x_o N/V$) for intercalates at the onset of superconductivity is inversely proportional to T_{c-o} . The appearance of a 'critical pressure' and its average value (~ 1 atm) seem to be the only empirical feature shared among intercalated superconductors reported to date.

This report delves into the emergence of superconductivity from perturbative methods beyond intercalation. It specifically investigates near onset conditions in (1) elemental superconductors, (2) doped compounds, and (3) pressurized compounds. Therefore, only a subset of superconductors, including the most cited/investigated, are analyzed out of the thousands in existence to date. Methods used in this

E-mail address: benjamin@magnet.fsu.edu

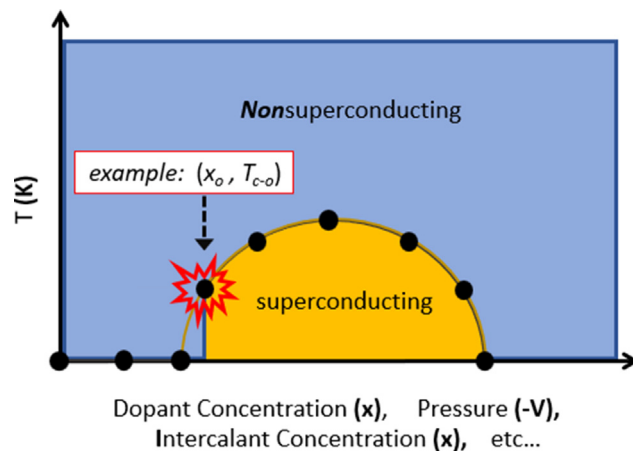


Fig. 1. Temperature versus atomic concentration x , pressurized unit cell volume V , and other control parameters, for a generic phase diagram depicting a nonsuperconducting region in blue and a dome-like superconducting region in gold. The highlighted onset point (x_o, T_{c-o}) is defined as the minimum perturbation (e.g., atomic concentration) required for superconductivity's emergence.

study do not apply to compounds like XTa_2S_5 [$\text{X} = \text{Mg, Ca, Sr, and Ba}$] [24–27] or MgB_2 [28] and $\text{Ba}_2\text{Nb}_3\text{S}_8\text{I}$ [29], which superconduct under iso electronic conditions or without obvious perturbations (chemical or physical) from a nonsuperconducting state, respectively. Investigated compounds include iron pnictides, cuprates, bismuth sulfides, nickelates, oxyhydrides, fluorides, and many others. Results are compared to onset conditions reported for intercalated compounds [22,23]. Comparisons involve the estimation of unit cell volumes (V) and onset perturbation densities (ρ_o) extracted from experimental data. Both parameters are then juxtaposed with onset transition temperatures (T_{c-o}). The onset perturbation density is defined as the minimum number of valence electrons (N) per formula unit per unit cell volume required for superconductivity to emerge from a nonsuperconducting compound. All data utilized in this manuscript have been sourced from previously reported experiments available on Google Scholar and are duly cited throughout the text.

2. Onset of elemental superconductivity

Empirical studies like those conducted by Matthias heavily influenced the direction of superconductivity research after the first superconductor was discovered in 1904 [30]. His work highlighted the importance of counting the total number of valence electrons a compound has per atom when attempting to predict new superconductors of particular structures or chemistries. Empirical rules regarding superconductivity evolving from particular synthesis pathways like intercalation, however, had not been discovered until recently, specifically in compounds of binary constituents and greater. This section now shifts focus to the onset of superconductivity in single-element compounds. To accomplish this, similar to the approach taken with intercalated compounds, we examine the nonsuperconducting/superconducting boundary within the periodic table of elements **as a function of increasing electron number** at standard temperature and pressure (STP). The landscape of known superconductors is vast and ever-growing. Nevertheless, it is important to underscore that unless a new element is discovered, the data set of single-element superconductors is uniquely complete as it represents 100% of superconductors known in their simplest chemical form to date.

Firstly, it is observed that a superconducting dome, akin to Fig. 1, is present in the periodic table of elements, as illustrated in Fig. 2. This depiction is constructed by initially considering group 1 elements

Na, K, Rb, Cs, and Fr, arranged here by increasing period number and depicted in blue squares in Fig. 2. These elements, each having one valence electron in their unfilled shell, do not exhibit superconductivity at STP. Superconductivity becomes evident at STP in Al, Ti, Zr, La, and Th, represented by gold squares with red borders in Fig. 2, only when 2 to 3 electrons are added to their unfilled shells and nucleons are adjusted accordingly. These elements signify the onset of superconductivity in shells $n = 3$ to $n = 7$, marking the initial boundary separating superconductors and nonsuperconductors as electrons increase from $N = 1$. Beyond this boundary and beneath the “dome” of superconductors shown in Fig. 2, nearly all elemental superconductors that exist at STP, excluding lithium and beryllium, are situated.

Calculated perturbation densities, $\rho_{elem.\#-o} = N_{elem.}/V$, for all 5 onset elements are shown in Table 1 and Fig. 3 (blue circles). The subscript “#” represents period number. Like intercalated systems (Fig. 3 – red circles), the distance correlation coefficient [31–32] for onset elements is high at $dCor(T_{c-o}, \rho_{elem.-o}) = .76$. For intercalates, $dCor(T_{c-o}, \rho_{int.-o}) = .62$. All distance coefficient calculations in this report were carried out with an in-house, self-designed, LabView VI utilizing algorithms reported by Szekely et al. [31].

A pressure $P_{elem.\#-o}$ (Eq. (2)) can be assigned to onset elements. For example, the pressure for Aluminum is $P_{elem.3-o} = 7.2$ atm, where $N = N_{elem.} = 3$, $V = 66.32 \text{ \AA}^3$, and $T_{c-o} = 1.175 \text{ K}$. Pressure estimates for onset elements and others are noted in Table 1. The average is 7.9 atm, as opposed to 1.3 atm for intercalated compounds. Arriving at the precise value of 1 atm for intercalates relies on the resolution and precision of the experimental data used in the analysis. Pressure estimates for elements wildly deviate from one another immediately beyond onset as shown in Table 1. See Table S1 in the supporting information section for similar analyses conducted on all superconductors located under the “dome” of superconductivity in Fig. 2.

$$P_{elem.\#-o} V = N \kappa T_{c-o} \quad (2)$$

Distance correlation coefficients for the relationship between T_{c-o} and V_o in onset elements and intercalates are shown in Fig. 4. They are .82 and .62, respectively. These values suggest T_{c-o} and V_o are highly correlated in onset elements and intercalates. Bear in mind, the periodic table also allows an examination of offset conditions. Transition temperatures in this scenario oscillate with unit cell volume (see supporting information), unlike monotonous $T_{c-o}(V)$. For intercalates, phase diagrams typically possess incomplete superconducting domes due to limitations in sample stability or synthesis methods. Therefore, offset conditions are not compared in this report.

3. Doping-induced superconductivity (non-isoelectronic)

An alternate route to chemically induce superconductivity is doping by single-element *substitution*. For instance, Yang et al. illustrated this with semimetallic IrTe_2 through intercalation and palladium doping. [11] The resultant compounds, Pd_xIrTe_2 and $\text{Ir}_{1-x}\text{Pd}_x\text{Te}_2$, with x_o equal to 0.02 and 0.03, respectively, provide unique insights into the initiation of superconductivity specific to the processes of doping and intercalation, given that the host and control parameter remain consistent in both cases.

Based on reported resistance measurements, both compounds exhibit onset transition temperatures of $T_{c-o} \approx 2.5 \text{ K}$. $\text{Pd}_{0.02}\text{IrTe}_2$, the intercalate, displays a narrower transition width. Yang et al. also demonstrated that the superconductivity in Pd_xIrTe_2 and $\text{Ir}_{1-x}\text{Pd}_x\text{Te}_2$ competes with density waves in a manner reminiscent of a quantum critical point. The calculated intercalation perturbation density $\rho_{int.-o}$ for $\text{Pd}_{x_o}\text{IrTe}_2$ is depicted in Fig. 3. The pressure inferred from Eq. (1) is approximately ~ 1 atm.

To search for correlated behavior in doping-induced superconductors we define a perturbation density in non-isoelectronically doped

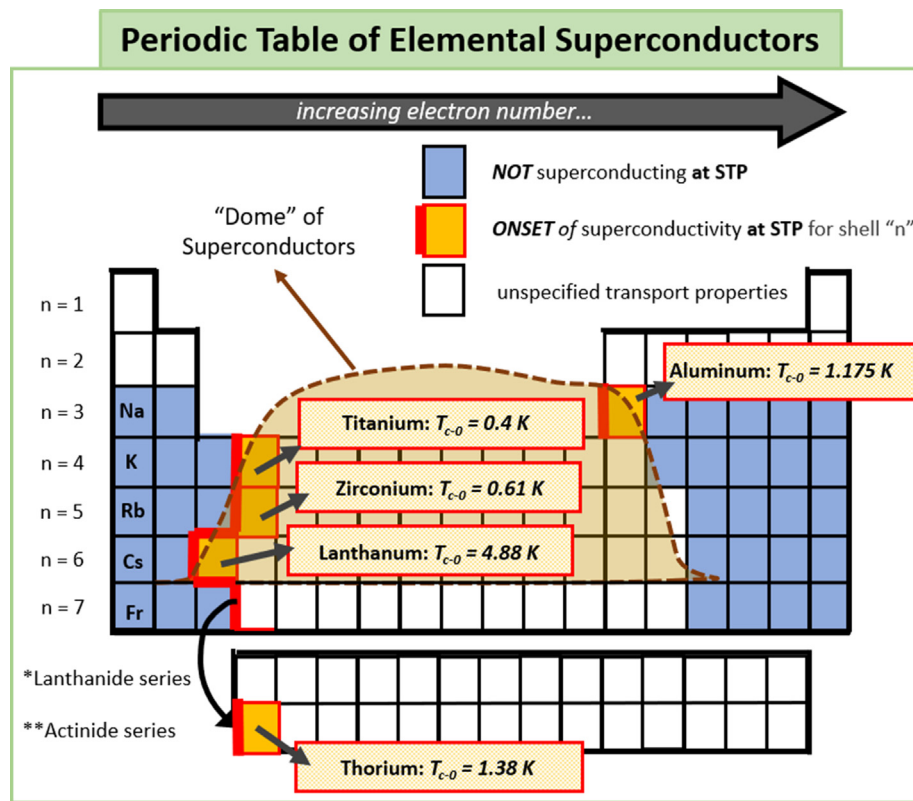


Fig. 2. Periodic table highlighting the onset of superconductivity in elements. The thick red borderline represents the boundary between nonsuperconducting elements and the onset of superconductivity within shells 3–7. Aluminum, Titanium, Zirconium, Lanthanum, and Thorium are the first elements to show superconductivity at STP as a function of increasing electron number in shells 3–7, respectively. They are shown in gold squares. Blue squares indicate elements showing no superconductivity at STP. White squares depict unspecified transport properties unless covered by the “Dome” of superconductors encapsulating most elements exhibiting superconductivity at STP.

Table 1

A list of nine elements which superconduct at STP. Bolded elements Al, Ti, Zr, La, and Th represent the onset of superconductivity in periods 3–7 (i.e., asterisked pressures). Elements V, Nb, Hf, and Pa are superconductors closest to onset in periods 4–7. Aluminum is the only superconductor at STP within n = 3.

Period (n)	[ref.] Element	T _c (K)	V (Å ³)	N _{elem.}	ρ _{elem.} (N _{elem.} /Å ³)	P (atm)
3	[33] Al	1.175	66.32	3	0.045	7.2*
4	[34] Ti	0.4	35.33	4	0.113	6.2*
4	[35] V	5.4	27.82	5	0.179	132.2
5	[36] Zr	0.61	46.56	4	0.0853	7.1*
5	[36] Nb	9.25	36.07	5	0.138	174.7
6	[37–38] La (α–β)	4.88–6.3	150.29	3	0.019–0.025	13.3–16.3*
6	[37] Hf	0.128	44.53	4	0.09	1.6
7	[37] Th	1.38	131.42	4	0.03	5.7*
7	[39] Pa	1.4	48.92	4	0.081	15.6

compounds as $\rho_{dop.-o} = x_o |\Delta N| / V$. The variable $|\Delta N|$ represents the difference in the number of outer electrons between elements under exchange. For $Ir_{1-x}Pd_xTe_2$ and most other compounds the value of $|\Delta N|$ is 1. An example compound having $|\Delta N| = 2$ is $SmFe_{1-x}Ni_xAsO$ [40]. The density is $4.14 \cdot 10^{26}$ electrons/m³ for $Ir_{1-x}Pd_xTe_2$ and it is plotted against T_{c-o} shown in Fig. 5 along with 70 other doped superconductors [9–11,40–100]. Unlike onset elements and intercalates, most of these materials exhibit both magnet and structural transitions near T_c . Therefore, the data are sorted into two categories. Grey squares represent sixteen compounds which do not show structural transitions (STR) near T_c ; all but two do not show magnetic transitions. Black squares represent fifty-six compounds which show structural transitions near T_c ; all but four also show magnetic transitions.

The average density is $3 \cdot 10^{26}$ electrons/m³ and nearly independent of T_{c-o} . The latter point is emphasized by the distance correlation

coefficient, $dCor(T_{c-o}, \rho_{dop.-o}) = .29$. It is even more evident in the histogram binned to $1 \cdot 10^{26}$ electrons/m³ shown in Fig. 6. The histogram is centered at $\sim 3 \cdot 10^{26}$ electrons/m³ and skewed to the right. Though a constant perturbation density is unexpected, its average value is reminiscent of current densities typically estimated via Hall measurements of the normal state in the vicinity of superconductivity. [101–103].

Notice correlations with temperature differ between $\rho_{int.-o}$ and $\rho_{dop.-o}$. The variable $\rho_{int.-o}$ is inversely proportional to T_{c-o} . If this correlation is also causal, it would imply the relevant itinerant electrons undergo a diffusive-type transport at the onset of intercalate superconductivity. This behavior mimics the typical transport behavior associated with intercalated systems like lithium-ion batteries [104], for example. The variable $\rho_{dop.-o}$ is weakly correlated to T_{c-o} . If causal, it implies a more non-diffusive (e.g., ballistic) type transport at the

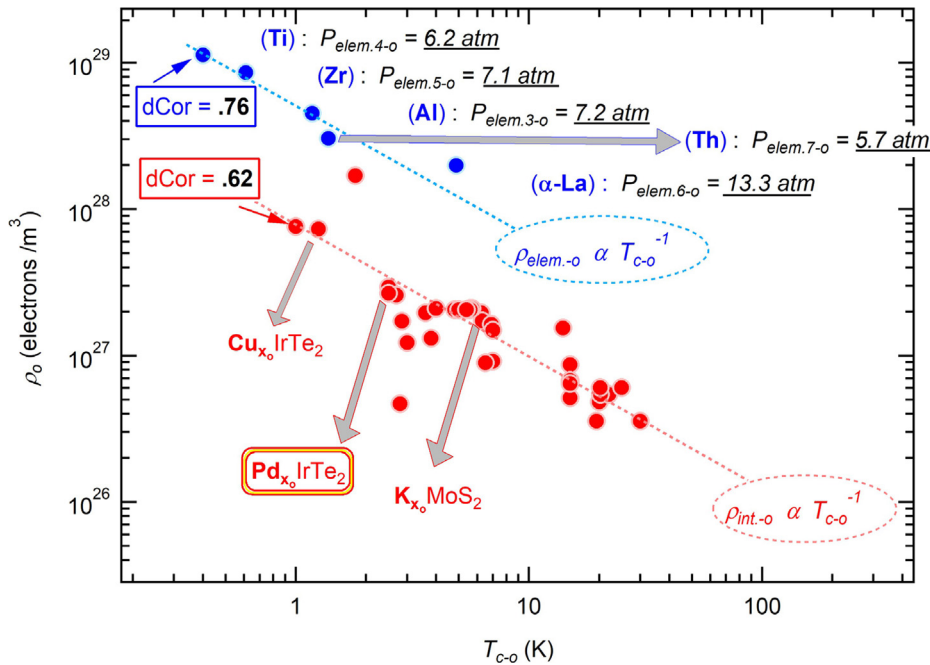


Fig. 3. Onset perturbation density, ρ_o , versus transition temperature, T_{c-o} . Blue circles represent data collected from 5 elemental superconductors [33,34,36–38]. The blue dotted line represents a guide to the eye showing $\rho_{elm.-o} \propto T^n$, where $n = -1$; it is not a fit of the data. A distance correlation coefficient of $dCor(T_{c-o}, \rho_{elm.-o}) = .76$ is indicated. Red circles represent data collected from forty-one intercalated superconductors. [6,11,22] The red dotted line represents a guide to the eye indicating $\rho_{int.-o} \propto T^n$, where $n = -1$; it is not a fit of the data. A distance correlation coefficient of $dCor(T_{c-o}, \rho_{int.-o}) = .62$ is indicated. The compounds $Cu_{x_o}IrTe_2$, $Pd_{x_o}IrTe_2$, and $K_{x_o}MoS_2$ are highlighted.

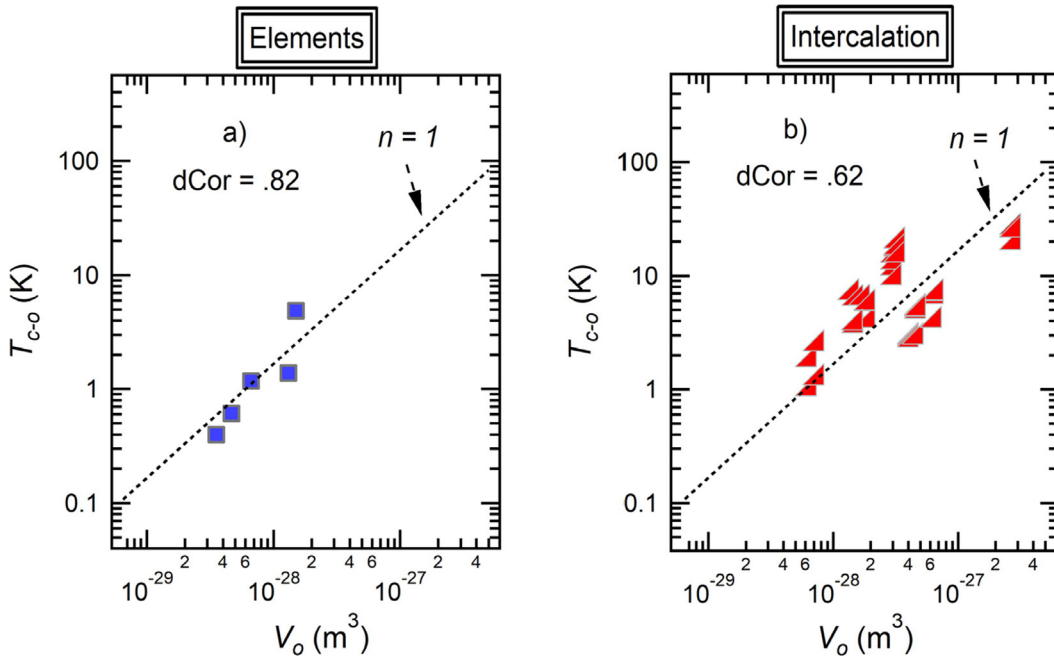


Fig. 4. Transition temperature, T_{c-o} , versus onset volume, V_o . Plot (a) depicts onset elements as blue squares with a distance correlation coefficient of .82 indicated. Dashed black line serves as a guide to the eye at $n = -1$ for $T_{c-o} \propto V^n$; it is not a fit of the data. Plot (b) depicts intercalates [6,11,22] as red triangles with a distance correlation coefficient of .62 indicated. Dashed black line serves as a guide to the eye at $n = -1$ for $T_{c-o} \propto V^n$; it is not a fit of the data.

onset of superconductivity in doped compounds for the assumed itinerant relevant electrons. These correlations and interpretation are supported by Yang et al.'s transport data for $Pd_{0.02}IrTe_2$ and $Ir_{0.97}Pd_{0.03}Te_2$ where it is evident that the intercalated compound's electrical resistance shows a greater temperature dependence during its transition to superconductivity. Also, according to their phase diagram, data

above onset suggests doped compounds are less affected by changes in electron density like our empirical result show in Fig. 5 for onset conditions. From their data, T_c in the doped remains nearly constant and persists well above onset ($x > 0.09$). For the intercalated, with similar perturbation, T_c peaks at $x = 0.03$ then quickly diminishes to almost non-existent at $x = 0.1$. This reveals the intimate connection

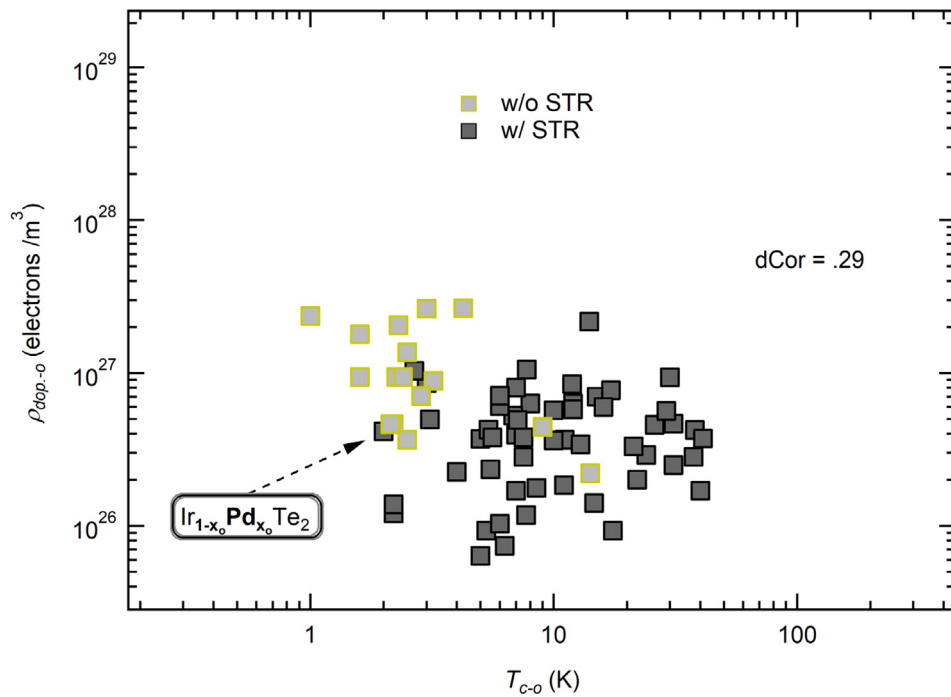


Fig. 5. Onset volumetric electron density, $\rho_{\text{dop},-o}$, versus transition temperature, $T_{c,-o}$. Grey and black squares represent data collected from seventy-one doped superconductors (see Table S2 in supporting information). The color difference partitions compounds into those which do (black) and do not (grey) exhibit structural transitions (STR), respectively. A distance correlation coefficient of $d\text{Cor}(T_{c,-o}, \rho_{\text{int},-o}) = .29$ is indicated. The compound $\text{Ir}_{1-x_0}\text{Pd}_{x_0}\text{Te}_2$ is highlighted.

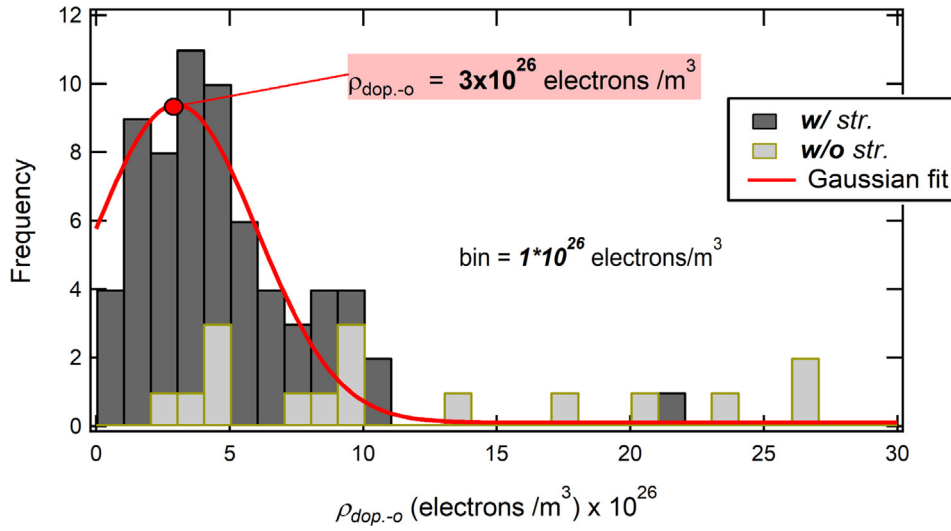


Fig. 6. Frequency of doped superconductors versus calculated onset valence electron density. Data from 71 doped superconductors (see Table S2 in supporting information) are displayed. Grey squares indicate doped superconductors which do show structural transitions, black squares indicate those which do not show structural transitions. Bin size is of width 1×10^{26} electrons/m³. The peak value of the gaussian fit is shown to be $\rho_{\text{dop},-o} = 3 \cdot 10^{26}$ electrons/m³.

between electron number density and T_c , like what is shown in Fig. 3 for onset intercalates. Summarized data comparing doping to intercalation are tabulated within Table S4 in supporting information.

Preceding sections have alluded to an ever-present critical pressure at the onset of superconductivity as a function of emergence pathways. Its origin was attributed to either the manifestation of Charles's law ($T \propto V$) or the observation that onset perturbation densities are inversely proportional to onset transition temperatures. On the contrary, neither of these situations appear relevant for doped compounds. Consequently, a similar ideal gas-like interpretation of critical pressure in doped superconductors, if it exists, seems unlikely. If a non-diffusive

critical pressure is to be assigned to the assumed itinerant onset electrons of doping-induced superconductors (i.e., $P_{\text{dop},-o}$), it would likely arise from the degeneracy pressure (i.e., $P_{\text{deg}} = P_{\text{dop},-o}$) created by these electrons, as shown in Eq. (3). The constants m_e and \hbar represent the electron mass and reduced Planck's constant, respectively. This implies a perturbation density of $\rho_{\text{dop},-o} = 3 \cdot 10^{26}$ electrons/m³ results in a critical pressure of $P_{\text{dop},-o} \approx 36$ atm.

$$P_{\text{deg.}} = \frac{\hbar^2}{5m_e} (3\pi^2)^{\frac{2}{3}} (\rho_{\text{dop},-o})^{\frac{5}{3}} \quad (3)$$

A way to uncover evidence of this presumed critical pressure is to examine the interface superconductivity of heterostructures formed by these compounds. Given Eqs. (3) and (1), the equation for T_c at the interface of an underdoped compound and an “onset” intercalated compound can be deduced. The condition $x_o|\Delta N| = x_oN_{int.-o}$ leads to a simple formula for T_c expressed in Eq. (4). This is intriguing as a T_c of approximately 29 K and/or its functional dependence on sample differences are not implausible attributes of unstrained interface superconductivity. [105–106] Eq. (5) illustrates the deduced T_c for the interface of an underdoped compound and an onset element. To date, the specific scenarios required for testing Eqs. (4) and (5) have not been reported.

$$T_{\text{interface}} = 29K \left(\frac{V_{int.-o}}{V_{dop.-o}} \right) \quad (4)$$

$$T_{\text{interface}} = 145K \left(\frac{V_{elem.-o}}{V_{dop.-o}} \right) \quad (5)$$

4. Discussion

The culmination of these results suggests high-temperature superconductivity favors dilute systems (i.e., $\rho_o \propto T^{-1}$) and large unit cell volumes (i.e., $T_{c-o} \propto V_o$) at the genesis of superconductivity. It also reveals a minimum real space density in many compounds displaying doping-induced superconductivity. It is important to note that these findings pertain to a section of the phase diagram requiring the least amount of chemical resources (i.e., onset) for the emergence of superconductivity. Therefore, this information may be crucial for the engineering of future low-cost high-temperature superconductors with less reliance on serendipity. Refer to empirical relationships summarized in Table 2.

As previously mentioned, pressurization is another pathway to superconductivity. Its effects are often likened to the “chemical pressure” associated with intercalation, for example [107–109]. Preliminary data we have observed in nearly 60 compounds [18,19,12–16,110–167] (see Table S3 in supporting information) also lend credence to this well-accepted idea concerning the relationship between T_{c-o} and V_o . Fig. 7 depicts data from compounds showing only a superconducting transition when cooled after pressurization, i.e., those possessing no magnetic ordering and no structural transitions. The distance correlation coefficient in this case is highly correlated at $dCor(V_o, T_{c-o}) = .8$. More work is needed to elucidate effects like magnetism on onset conditions in pressurized compounds; see Fig. S1 in supporting information for further analysis.

5. Conclusion

Correlated behavior has been identified near the onset of superconductivity in systematically tuned compounds with nuanced considerations of V , N , and T_c . In addition to contributing to fundamental research efforts, the author aims for this investigation to aid in refining

Table 2

Summary of empirical equations at the onset of superconductivity in intercalates, single-elements, and doped compounds.

Synthesis Technique	Empirical Observation (1 K < T_c < 40 K)	Critical Pressure (1 K < T_c < 40 K)
Intercalation	$\rho_{int.-o} \propto T_{c-o}^{-1}$	~1.3 atm
Single Elements	$\rho_{elem.-o} \propto T_{c-o}^{-1}$	~6.5 atm*
Doping	$\rho_{dop.-o} \approx \text{constant}$	~36 atm**

* For shells $n \geq 3$, La: 13.3 atm.

** If related to Fermi/degeneracy pressure.

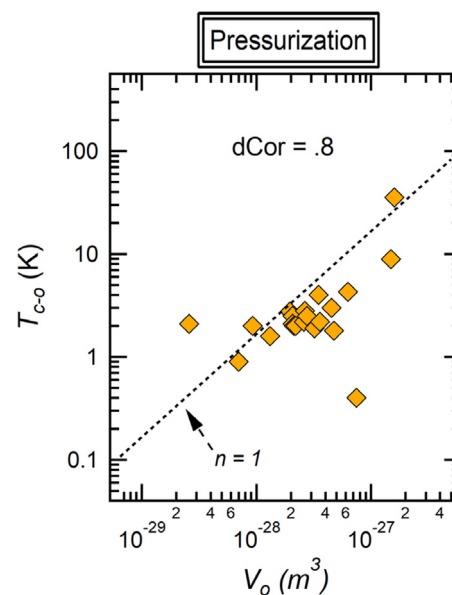


Fig. 7. Onset transition temperature, T_{c-o} , versus onset unit cell volume, V_o for 20 pressure-induced superconductors (see Table S3 in supporting information). A distance correlation coefficient of $dCor(V_o, T_{c-o}) = .8$ is indicated. Dashed line indicates $n = 1$ as a guide to the eye for $T_{c-o} \propto V_o^n$; it is not a fit of the data.

the physical and chemical phase space explored by the scientific community in their quest for new and innovative superconductors.

Funding

The National High Magnetic Field Laboratory is supported by the National Science Foundation through NSF/DMR-2128556, NSF/DMR-1644779, and the State of Florida.

CRediT authorship contribution statement

Shermane M. Benjamin: Conceptualization, Data curation, Formal analysis, Investigation, Methodology, Project administration, Supervision, Validation, Visualization, Writing – original draft, Writing – review & editing.

Declaration of competing interest

The authors declare that they have no known competing financial interests or personal relationships that could have appeared to influence the work reported in this paper.

Acknowledgements

The author sincerely thanks P.M. Eugenio, J. Jaroszynski, T. Murphy, M. Ozerov, M. Lee, B. Casas, D. Chichinadze, R. Baumbach, L. Balicas, C. Moir, D. Graf, E.S. Choi, and L. Nelson for many useful discussions. The author also expresses their gratitude to the reviewers and editor for their comments and critiques toward significantly improving the manuscript.

Appendix A. Supplementary material

Supplementary material to this article can be found online at <https://doi.org/10.1016/j.supcon.2024.100098>.

References

- [1] Sajadi E, Palomaki T, Fei Z, Zhao W, Bement P, Olsen C, et al. Gate-induced superconductivity in a monolayer topological insulator. *Science* 2018;362:922–5.
- [2] Costanzo D, Jo S, Berger H, Morpurgo AF. Gate-induced superconductivity in atomically thin MoS₂ crystals. *Nat Nanotechnol* 2016;11:339–44.
- [3] Saito Y, Nojima T, Iwasa Y. Gate-induced superconductivity in two-dimensional atomic crystals. *Supercond Sci Technol* 2016;29:093001.
- [4] Rhodes DA et al. Enhanced Superconductivity in monolayer T_d-MoTe₂. *Nano Lett* 2021;21:2505–11.
- [5] Cao Y, Fatemi V, Fang S, Watanabe K, Taniguchi T, Kaxiras E, et al. Unconventional superconductivity in magic-angle graphene superlattices. *Nature* 2018;556:43–50.
- [6] Neu J, Graf D, Wei K, Gaiser A, Xin Y, Lai Y, et al. Superstructures and superconductivity linked with Pd intercalation in Nb₂Pd_xSe₅. *Chem Mater* 2020;32:8361–6.
- [7] Morosan E, Zandbergen HW, Dennis BS, Bos JWG, Onose Y, Klimczuk T, et al. Superconductivity in Cu_xTiSe₂. *Nat Phys* 2006;2:544–50.
- [8] Zhang R, Tsai I-L, Chapman J, Khestanova E, Waters J, Grigorieva IV. Superconductivity in potassium-doped metallic polymorphs of MoS₂. *Nano Lett* 2016;16:629–36.
- [9] Hu R, Bud'ko SL, Straszheim WE, Canfield PC. Phase diagram of superconductivity and antiferromagnetism in single crystals of Sr(Fe_{1-x}Co_x)₂As₂ and Sr_{1-y}Eu_y(Fe_{0.88}Co_{0.12})₂As₂. *Phys Rev B* 2011;83:094520.
- [10] Takagi H, Ido T, Ishibashi S, Uota M, Uchida S, Tokura Y. Superconductor-to-nonsuperconductor transition in (La_{1-x}Sr_x)₂CuO₄ as investigated by transport and magnetic measurements. *Phys Rev B* 1989;40:2254–61.
- [11] Yang JJ, Choi YJ, Oh YS, Hogan A, Horibe Y, Kim K, et al. Charge-orbital density wave and superconductivity in the strong spin-orbit coupled IrTe₂: Pd. *Phys Rev Lett* 2012;108:116402.
- [12] Mani A, Ghosh N, Paulraj S, Bharathi A, Sundar CS. Pressure-induced superconductivity in BaFe₂As₂ single crystal. *Europhys Lett* 2009;87:17004.
- [13] Mathur ND, Grosche FM, Julian SR, Walker IR, Freye DM, Haselwimmer RKW, et al. Magnetically mediated superconductivity in heavy fermion compounds. *Nature* 1998;394:39–43.
- [14] Zhang JL et al. Pressure-induced superconductivity in topological parent compound Bi₂Te₃. *Proc Natl Acad Sci* 2011;108:24–8.
- [15] Drozdov AP, Kong PP, Minkov VS, Besedin SP, Kuzovnikov MA, Mozaffari S, et al. Superconductivity at 250 K in lanthanum hydride under high pressures. *Nature* 2019;569:528–31.
- [16] Kong P, Minkov VS, Kuzovnikov MA, Drozdov AP, Besedin SP, Mozaffari S, et al. Superconductivity up to 243 K in the yttrium-hydrogen system under high pressure. *Nat Commun* 2021;12:5075.
- [17] Drozdov AP, Eremets MI, Troyan IA, Ksenofontov V, Shylin SI. Conventional superconductivity at 203 kelvin at high pressures in the sulfur hydride system. *Nature* 2015;525:73–6.
- [18] Li X, Sun J, Shahi P, Gao M, MacDonald AH, Uwatoko Y, et al. Pressure-induced phase transitions and superconductivity in a black phosphorus single crystal. *Proc Natl Acad Sci* 2018;115:9935–40.
- [19] Shen X, Ma H, Bhoi D, Gouchi J, Uwatoko Y, Dalan A, et al. Pressure induced superconductivity and multiple structural transitions in CsCl-Type Cubic CeZn single crystal. *Crystals* 2022;12:571.
- [20] Li L, Richter C, Mannhart J, Ashoori RC. Coexistence of magnetic order and two-dimensional superconductivity at LaAlO₃/SrTiO₃ interfaces. *Nat Phys* 2011;7:762–6.
- [21] Drew AJ et al. Coexistence of static magnetism and superconductivity in SmFeAsO_{1-x}F_x as revealed by muon spin rotation. *Nat Mater* 2009;8:310–4.
- [22] Benjamin SM. Estimating the single-element concentration of intercalated insulators for the emergence of superconductivity. *ACS Phys Chem Au* 2022;2:108–17.
- [23] Benjamin SM. Intercalate superconductivity and van der Waals Equation. *ACS Mater Au* 2022;2:436–9.
- [24] Benjamin SM, Rieders NF, Smith MG, Neumeier JJ. From Ta₂S₅ Wires to Ta₂O₅ and Ta₂O_{5-x}S_x. *ACS Omega* 2021;6:5445–50.
- [25] Benjamin SM, Smith MG, Neumeier JJ. Superconductivity in MgTa₂S₅. *Physica C* (Amsterdam, Neth) 2021;1353966.
- [26] Drenner AK, Benjamin SM, Smith MG, Neumeier JJ. Physical properties and superconductivity of SrTa₂S₅. *Physica C* (Amsterdam, Neth) 2019;556:19–23.
- [27] Drenner AK, Benjamin SM, Smith MG, Neumeier JJ. Physical properties and superconductivity of BaTa₂S₅. *Physica C* (Amsterdam, Neth) 2019;566:1353522.
- [28] Choi HJ, Roundy D, Sun H, Cohen ML, Louie SG. The origin of the anomalous superconducting properties of MgB₂. *Nature* 2002;418:758–60.
- [29] Smith MG, Lin Q, Benjamin SM, Baker MT, Neumeier JJ. Crystal structure and physical properties of Ba₂Nb₃S₈: A new misfit-layered transition-metal dichalcogenide superconductor. *J Phys Chem Solid* 2021;156:110135.
- [30] Matthias BT. Empirical relation between superconductivity and the number of valence electrons per atom. *Phys Rev* 1955;97:74–6.
- [31] Székely GJ, Rizzo ML, Bakirov NK. Measuring and testing dependence by correlation of distances. *Ann Stat* 2007;35:2769–94.
- [32] Székely GJ, Rizzo ML. Brownian distance covariance. *Ann Appl Stat* 2009;3:1236–65. Publisher Institute of Mathematical Statistics.
- [33] Caplan S, Chanin G. Critical-field study of superconducting aluminum. *Phys Rev* 1965;138:A1428–33.
- [34] Steele MC, Hein RA. Superconductivity of titanium. *Phys Rev* 1953;92:243–7.
- [35] Wexler A, Corak WS. Superconductivity of vanadium. *Phys Rev* 1952;85:85–90.
- [36] Eisenstein J. Superconducting elements. *Rev Mod Phys* 1954;26:277–91.
- [37] Matthias BT, Geballe TH, Compton VB. Superconductivity. *Rev Mod Phys* 1963;35:1–22.
- [38] Debessai M, Hamlin JJ, Schilling JS. Comparison of the pressure dependences of T_c in the trivalent d-electron superconductors Sc, Y, La, and Lu up to megabar pressures. *Phys Rev B* 2008;78:064519.
- [39] Fowler RD, Matthias BT, Asprey LB, Hill HH, Lindsay JDG, Olsen CE, et al. Superconductivity of protactinium. *Phys Rev Lett* 1965;15:860–2.
- [40] Li YK, Lin X, Zhou T, Shen Q, Tao Q, Cao GH, et al. Superconductivity induced by Ni doping in SmFe_{1-x}Ni_xAs_{0.5}. *J Phys Condens Matter* 2009;21:355702.
- [41] Zhang Y et al. Unusual doping dependence of the electronic structure and Co-existence of spin-density-wave and superconductor phases in single crystalline Sr_{1-x}K_xFe₂As₂. *Phys Rev Lett* 2009;102:127003.
- [42] Gen-Fu C, Zheng L, Gang L, Wan-Zheng H, Jing D, Jun Z, et al. Superconductivity in hole-doped (Sr_{1-x}K_x)Fe₂As₂. *Chin Phys Lett* 2008;25:3403.
- [43] Hiramatsu H, Katase T, Kamiya T, Hosono H. Superconducting properties and phase diagram of indirectly electron-doped Sr_{1-x}La_xFe₂As₂ epitaxial films grown by pulsed laser deposition. *IEEE Trans Appl Supercond* 2013;23:7300405.
- [44] Taddei KM, Allred JM, Bugaris DE, Lapidus SH, Krogstad MJ, Claus H, et al. Observation of the magnetic C₄ phase in Ca_{1-x}Na_xFe₂As₂ and its universality in the hole-doped 122 superconductors. *Phys Rev B* 2017;95:064508.
- [45] Han F, Zhu X, Cheng P, Mu G, Jia Y, Fang L, et al. Superconductivity and phase diagrams of the 4d- and 5d-metal-doped iron arsenides SrFe_{2-x}M_xAs₂ (M = Rh, Ir, Pd). *Phys Rev B* 2009;80:024506.
- [46] Saha SR, Butch NP, Kirshenbaum K, Paglione J. Evolution of bulk superconductivity in SrFe₂As₂ with Ni substitution. *Phys Rev B* 2009;79:224519.
- [47] Hardy F, Burger P, Wolf T, Fisher RA, Schweiss P, Adelmann P, et al. Doping evolution of superconducting gaps and electronic densities of states in Ba(Fe_{1-x}Co_x)₂As₂ iron pnictides. *Europhys Lett* 2010;91:47008.
- [48] Canfield PC, Bud'ko SL, Ni N, Yan JQ, Kracher A. Decoupling of the superconducting and magnetic/structural phase transitions in electron-doped BaFe₂As₂. *Phys Rev B* 2009;80:060501.
- [49] Ni N, Thaler A, Kracher A, Yan JQ, Bud'ko SL, Canfield PC. Phase diagrams of Ba(Fe_{1-x}M_x)₂As₂ single crystals (M = Rh and Pd). *Phys Rev B* 2009;80:024511.
- [50] Katase T, Hiramatsu H, Kamiya T, Hosono H. Magnetic scattering and electron pair breaking by rare-earth-ion substitution in BaFe₂As₂ epitaxial films. *New J Phys* 2013;15:073019.
- [51] Chen H, Ren Y, Qiu Y, Bao W, Liu RH, Wu G, et al. Coexistence of the spin-density wave and superconductivity in Ba_{1-x}K_xFe₂As₂. *Europhys Lett* 2009;85:17006.
- [52] Yamagishi T, Ueda S, Takeda S, Takano S, Mitsuda A, Naito M. A study of the doping dependence of T_c in Ba_{1-x}K_xFe₂As₂ and Sr_{1-x}K_xFe₂As₂ films grown by molecular beam epitaxy. *Physica C* (Amsterdam, Neth) 2011;471:1177–80.
- [53] Oner Y, Boyraz C, Hiramatsu H, Katase T, Hosono H. Coexistence of magnetism and superconductivity in thin films of the Fe-based superconductor Ba_{1-x}La_xFe₂As₂. *J Phys Condens Matter* 2020;32:485804.
- [54] Avci S, Allred JM, Chmaisssem O, Chung DY, Rosenkranz S, Schlüter JA, et al. Structural, magnetic, and superconducting properties of Ba_{1-x}Na_xFe₂As₂. *Phys Rev B* 2013;88:094510.
- [55] Peschke S, Stürzer T, Johrendt D. Ba_{1-x}Rb_xFe₂As₂ and generic phase behavior of hole-doped 122-type superconductors. *Zeitschrift für anorganische und allgemeine Chemie* 2014;640:830–5.
- [56] Cui J, Roy B, Tanatar MA, Ran S, Bud'ko SL, Prozorov R, Canfield PC, Furukawa Y. Antiferromagnetic spin correlations and pseudogaplike behavior in Ca(Fe_{1-x}Co_x)₂As₂ studied by 75As nuclear magnetic resonance and anisotropic resistivity. *Phys Rev B* 2015;92:184504.
- [57] Ran S, Bud'ko SL, Straszheim WE, Soh J, Kim MG, Kreyssig A, Goldman AI, Canfield PC. Control of magnetic, nonmagnetic, and superconducting states in annealed Ca(Fe_{1-x}Co_x)₂As₂. *Phys Rev B* 2012;85:224528.
- [58] Zhou W, Shi ZX. Review on origin of the unusual high-T_c superconductivity in Ca_{1-x}RE_xFe₂As₂ (RE = La, Ce, Pr, Nd). *Novel Supercond Mater* 2015;1:15–23.
- [59] Saha SR, Butch NP, Drye T, Magill J, Ziemak S, Kirshenbaum K, et al. Structural collapse and superconductivity in rare-earth-doped CaFe₂As₂. *Phys Rev B* 2012;85:024525.
- [60] Gao B, Li X, Ji Q, Mu G, Li W, Hu T, et al. Phase diagram and weak-link behavior in Nd-doped CaFe₂As₂. *New J Phys* 2014;16:113024.
- [61] Qi Y, Wang L, Gao Z, Wang D, Zhang X, Wang C, et al. Superconductivity induced by doping Rh in CaFe_{2-x}Rh_xAs₂. *New J Phys* 2011;13:033020.
- [62] Liu Y-B, Liu Y, Cui Y-W, Wu S-Q, Ren Z, Cao G-H. Magnetic and superconducting phase diagram of Eu(Fe_{1-x}Ni_x)As₂. *Phys Rev B* 2021;104:014501.
- [63] Anupam, Paulose PL, Ramakrishnan S, Hossain Z. Doping dependent evolution of magnetism and superconductivity in Eu_{1-x}K_xFe₂As₂ (x = 0–1) and temperature dependence of the lower critical field H_{c1}. *J Phys Condens Matter* 2011;23:455702.
- [64] Deguchi K, Mizuguchi Y, Demura S, Hara H, Watanabe T, Denholme SJ, et al. Evolution of superconductivity in LaO_{1-x}F_xBi₂ prepared by high-pressure technique. *Europhys Lett* 2013;101:17004.
- [65] Yazici D, Huang K, White BD, Jeon I, Burnett VW, Friedman AJ, et al. Superconductivity induced by electron doping in La_{1-x}M_xOBiS₂ (M = Ti, Zr, Hf, Th). *Phys Rev B* 2013;87:174512.
- [66] Jha R, Awana VPS. Superconducting properties of BiS₂-based superconductor NdO_{1-x}F_xBiS₂ (x = 0 to 0.9). *Mater Res Express* 2014;1:016002.
- [67] Jha R, Kishan H, Awana VPS. Superconducting and magneto-transport properties of BiS₂ based superconductor PrO_{1-x}F_xBiS₂ (x = 0 to 0.09). *J Appl Phys* 2014;115:013902.
- [68] Li Y, Lin X, Li L, Zhou N, Xu X, Cao C, et al. Electronic phase diagram in a new BiS₂-based Sr_{1-x}La_xFBiS₂ system. *Supercond Sci Technol* 2014;27:035009.

- [69] Lin X, Ni X, Chen B, Xu X, Yang X, Dai J, et al. Superconductivity induced by La doping in $\text{Sr}_{1-x}\text{La}_x\text{FeBi}_2$. *Phys Rev B* 2013;87:020504.
- [70] Demura S et al. Coexistence of bulk superconductivity and magnetism in $\text{CeO}_{1-x}\text{F}_x\text{Bi}_2$. *J Phys Soc Jpn* 2015;84:024709.
- [71] Xing J, Li S, Ding X, Yang H, Wen H-H. Superconductivity appears in the vicinity of semiconducting-like behavior in $\text{CeO}_{1-x}\text{F}_x\text{Bi}_2$. *Phys Rev B* 2012;86:214518.
- [72] Wang C, Li YK, Zhu ZW, Jiang S, Lin X, Luo YK, et al. Effects of cobalt doping and phase diagrams of $\text{LFe}_{1-x}\text{Co}_x\text{AsO}$ ($L = \text{La}$ and Sm). *Phys Rev B* 2009;79:054521.
- [73] Cao G, Jiang S, Lin X, Wang C, Li Y, Ren Z, et al. Narrow superconducting window in $\text{LaFe}_{1-x}\text{Ni}_x\text{AsO}$. *Phys Rev B* 2009;79:174505.
- [74] Wen H-H, Mu G, Fang L, Yang H, Zhu X. Superconductivity at 25 K in hole-doped $\text{La}_{1-x}\text{Sr}_x\text{FeAs}$. *Europhys Lett* 2008;82:17009.
- [75] Prando G, Vakaliuk O, Sanna S, Lamura G, Shiroka T, Bonfa P, et al. Role of in-plane and out-of-plane dilution in CeFeAsO: Charge doping versus disorder. *Phys Rev B* 2013;87:174519.
- [76] Shang T, Jiao L, Dai J, Yuan HQ, Balakirev FF, Hu WZ, et al. Robust magnetic order of Ce 4f-electrons coexisting with superconductivity in CeFeAsO_{1-x}F_x. *J Korean Phys Soc* 2013;62:2001–3.
- [77] Chen YL, Cheng CH, Cui YJ, Zhang H, Zhang Y, Yang Y, et al. Ir doping-induced superconductivity in the SmFeAsO system. *J Am Chem Soc* 2009;131:10338–9.
- [78] Chen GF, Li Z, Wu D, Li G, Hu WZ, Dong J, et al. Superconductivity at 41 K and its competition with spin-density-wave instability in layered $\text{CeO}_{1-x}\text{F}_x\text{FeAs}$. *Phys Rev Lett* 2008;100:247002.
- [79] Cui YJ, Chen YL, Cheng CH, Yang Y, Jiang J, Wang YZ, et al. Superconductivity and magnetism in Ir-doped GdFeAsO. *Physica C* (Amsterdam, Neth) 2010;470:1077–80.
- [80] Dunsiger SR, Zhao Y, Yamani Z, Buyers WJL, Dabkowska HA, Gaulin BD. Incommensurate spin ordering and fluctuations in underdoped $\text{La}_{2-x}\text{Ba}_x\text{CuO}_4$. *Phys Rev B* 2008;77:224410.
- [81] Hücker M, Zimmermann MV, Gu GD, Xu ZJ, Wen JS, Xu G, Kang HJ, Zheludev A, Tranquada JM. Stripe order in superconducting $\text{La}_{2-x}\text{Ba}_x\text{CuO}_4$ ($0.095 \leq x \leq 0.155$). *Phys Rev B* 2011;83:104506.
- [82] Krockenberger Y, Kurian J, Winkler A, Tsukada A, Naito M, Alff L. Superconductivity phase diagrams for the electron-doped cuprates $R_{2-x}\text{Ce}_x\text{CuO}_4$ ($R = \text{La}, \text{Pr}, \text{Nd}, \text{Sm}$, and Eu). *Phys Rev B* 2008;77:060505.
- [83] Fujita M, Kubo T, Kuroshima S, Uefuji T, Kawashima K, Yamada K, et al. Magnetic and superconducting phase diagram of electron-doped $\text{Pr}_{1-x}\text{LaCe}_x\text{CuO}_4$. *Phys Rev B* 2003;67:014514.
- [84] Kawashima Y, Ichimura K, Katono K, Kurosawa T, Oda M, Tanda S, et al. STM/STS study of the superconducting gap in SmFeAsO_{1-x}F_x. *Solid State Commun* 2015;204:33–6.
- [85] Cui YJ, Chen YL, Cheng CH, Yang Y, Wang YZ, Li YC, et al. Preparation of REFeAsO_{1-x}F_x (RE=Sm and Gd) superconductors at a relatively low temperature. *J Phys Chem Solid* 2011;72:449–52.
- [86] Hanna ARN, Abdel-Hafez M. Single-crystal growth and small anisotropy of the lower critical field in oxypnictides: NdFeAsO_{1-x}F_x. *Crystals* 2020;10:362.
- [87] Rotundu CR, Keane DT, Freelon B, Wilson SD, Kim A, Valdivia PN, et al. Phase diagram of the PrFeAsO_{1-x}F_x superconductor. *Phys Rev B* 2009;80:144517.
- [88] Kamihara Y, Watanabe T, Hirano M, Hosono H. Iron-based layered superconductor $\text{La}[\text{O}_{1-x}\text{F}_x]\text{FeAs}$ ($x = 0.05\text{--}0.12$) with $T_c = 26$ K. *J Am Chem Soc* 2008;130:3296–7.
- [89] Takahashi H, Soeda H, Nukii M, Kawashima C, Nakanishi T, Iimura S, et al. Superconductivity at 52 K in hydrogen-substituted $\text{LaFeAsO}_{1-x}\text{H}_x$ under high pressure. *Sci Rep* 2015;5:7829.
- [90] Osada M, Wang BY, Lee K, Li D, Hwang HY. Phase diagram of infinite layer praseodymium nickelate $\text{Pr}_{1-x}\text{Sr}_x\text{NiO}_2$ thin films. *Phys Rev Mater* 2020;4:121801.
- [91] Osada M, Wang BY, Goodge BH, Harvey SP, Lee K, Li D, et al. Nickelate superconductivity without rare-earth magnetism: $(\text{La}, \text{Sr})\text{NiO}_2$. *Adv Mater* 2021;33:2104083.
- [92] Zeng S et al. Phase diagram and superconducting dome of infinite-layer $\text{Nd}_{1-x}\text{Sr}_x\text{NiO}_2$ thin films. *Phys Rev Lett* 2020;125:147003.
- [93] Li D, Wang BY, Lee K, Harvey SP, Osada M, Goodge BH, et al. Superconducting dome in $\text{Nd}_{1-x}\text{Sr}_x\text{NiO}_2$ infinite layer films. *Phys Rev Lett* 2020;125:027001.
- [94] Karimoto S, Ueda K, Naito M, Imai T. Superconducting thin films of electron-doped infinite-layer $\text{Sr}_{1-x}\text{La}_x\text{CuO}_2$ grown by molecular beam epitaxy. *Physica C* 2002;378:381–30.
- [95] Kim M et al. Superconductivity in $(\text{Ba}, \text{K})\text{Sb}_3$. *Nat Mater* 2022;21:627–33.
- [96] Pei S, Jorgensen JD, Dabrowski B, Hinks DG, Richards DR, Mitchell AW, et al. Structural phase diagram of the $\text{Ba}_{1-x}\text{K}_x\text{BiO}_3$ system. *Phys Rev B* 1990;41:4126–41.
- [97] Doan P, Gooch M, Tang Z, Lorenz B, Möller A, Tapp J, Chu PCW, Guloy AM. $\text{Ba}_{1-x}\text{Na}_2\text{Ti}_2\text{Sb}_2\text{O}$ ($0.0 \leq x \leq 0.33$): A layered titanium-based pnictide oxide superconductor. *J Am Chem Soc* 2012;134:16520–3.
- [98] Ohishi K, Yamada I, Koda A, Higemoto W, Saha SR, Kadono R, Kojima KM, Azuma M, Takano M. Magnetic phase diagram of hole-doped $\text{Ca}_{2-x}\text{Na}_x\text{CuO}_2\text{Cl}_2$ cuprate superconductor. *J Phys Soc Jpn* 2005;74:2408–12.
- [99] Li LJ, Lu WJ, Zhu XD, Ling LS, Qu Z, Sun YP. Fe-doping-induced superconductivity in the charge-density-wave system 1T-TaS₂. *Europhys Lett* 2012;97:67005.
- [100] Pyon S, Kudo K, Nohara M. Superconductivity induced by bond breaking in the triangular lattice of IrTe₂. *J Phys Soc Jpn* 2012;81:053701.
- [101] Bhattacharyya A, Adroja DT, Hillier AD, Jha R, Awana VPS, Strydom AM. Superconducting gap structure in the electron doped BiS₂-based superconductor. *J Phys Condens Matter* 2017;29:265602.
- [102] Leng H, Cherian D, Huang YK, Orain J-C, Amato A, de Visser A. Muon spin rotation study of the topological superconductor $\text{Sr}_x\text{Bi}_2\text{Se}_3$. *Phys Rev B* 2018;97. Publisher: American Physical Society.
- [103] Zhou Q, Rhodes D, Zhang QR, Tang S, Schönenmann R, Balicas L. Hall effect within the colossal magnetoresistive semimetallic state of MoTe₂. *Phys Rev B* 2016;94:121101.
- [104] Goodenough JB, Park K-S. The Li-ion rechargeable battery: A perspective. *J Am Chem Soc* 2013;135:1167–76.
- [105] Yang H, Zhou G, Zhu Y, Gong G-M, Zhang Q, Liao M, et al. Superconductivity above 28 K in single unit cell FeSe films interfaced with $\text{GaO}_2\delta$ layer on NdGaO₃(110). *Sci Bull* 2019;64:490–4.
- [106] Qin H, Chen X, Guo B, Pan T, Zhang M, Xu B, et al. Moiré superlattice-induced superconductivity in one-unit-cell FeTe. *Nano Lett* 2021;21:1327–34.
- [107] Lin K, Li Q, Yu R, Chen J, Paul Attfield J, Xing X. Chemical pressure in functional materials. *Chem Soc Rev* 2022;51:5351–64.
- [108] Guo J, Lei H, Hayashi F, Hosono H. Superconductivity and phase instability of NH₃-free Na-intercalated FeSe_{1-z}S_z. *Nat Commun* 2014;5:4756.
- [109] Rajapakse M, Karki B, Abu O, Pishgar S, Musa MRK, Riyadh SMS, et al. Intercalation as a versatile tool for fabrication, property tuning, and phase transitions in 2D materials. *npj 2D Mater Appl* 2021;5:1–21.
- [110] Kikegawa T, Iwasaki H. An X-ray diffraction study of lattice compression and phase transition of crystalline phosphorus. *Acta Crystallogr B* 1983;39:158–64.
- [111] Zhen J, Deng W, Li C, Feng J, Zhang S, Wan S, et al. Superconductivity in In_2Te_3 under compression induced by electronic and structural phase transitions. *J Phys Chem Lett* 2022;13:1226–33.
- [112] Hung TL, Huang CH, Deng LZ, Ou MN, Chen YY, Wu MK, et al. Pressure induced superconductivity in MnSe. *Nat Commun* 2021;12:5436.
- [113] Wang S, Chen X, An C, Zhou Y, Zhou Y, Gu C, et al. Pressure-induced superconductivity in the quasi-one-dimensional charge density wave material CuTe. *Phys Rev B* 2021;103:134518.
- [114] Chi Z, Chen X, Yen F, Peng F, Zhou Y, Zhu J, et al. Superconductivity in pristine $2\text{H}_d\text{MoS}_2$ at ultrahigh pressure. *Phys Rev Lett* 2018;120:037002.
- [115] Zhou Y et al. Pressure-induced superconductivity in a three-dimensional topological material ZrTe_5 . *Proc Natl Acad Sci* 2016;113:2904–9.
- [116] Li X et al. Pressure-induced phase transitions and superconductivity in a quasi-1-dimensional topological crystalline insulator $\alpha\text{-Bi}4\text{Br}_4$. *Proc Natl Acad Sci* 2019;116:17696–700.
- [117] Marini G, Barone P, Sanna A, Tresea C, Benfatto L, Profeta G. Superconductivity in tin selenide under pressure. *Phys Rev Mater* 2019;3:114803.
- [118] Kong PP, Zhang JL, Zhang SJ, Zhu J, Liu QQ, Yu RC, et al. Superconductivity of the topological insulator Bi_2Se_3 at high pressure. *J Phys Condens Matter* 2013;25:362204.
- [119] Cai W, Lin W, Li L-H, Mallikas CD, Zhang R, Groesbeck M, et al. Pressure-induced superconductivity and flattened Se₆ rings in the wide band gap semiconductor $\text{Cu}_{2,2}\text{Se}_6$. *J Am Chem Soc* 2019;141:15174–82.
- [120] Wang Y, Ying J, Zhou Z, Sun J, Wen T, Zhou Y, et al. Emergent superconductivity in an iron-based honeycomb lattice initiated by pressure-driven spin-crossover. *Nat Commun* 2014;2018:9.
- [121] Pei C, Jin S, Huang P, Vymazalova A, Gao L, Zhao Y, et al. Pressure-induced superconductivity and structure phase transition in Pt_2HgSe_3 . *npj Quantum Mater* 2021;6:1–8.
- [122] Matsumoto R, Song P, Adachi S, Saito Y, Hara H, Yamashita A, et al. Pressure-induced superconductivity in tin sulfide. *Phys Rev B* 2019;99:184502.
- [123] Ehm L, Knorr K, Dera P, Krimmel A, Bouvier P, Mezouar M. Pressure-induced structural phase transition in the IV-VI semiconductor SnS. *J Phys Condens Matter* 2004;16:3545.
- [124] Malavi P, Paul A, Bera A, Muthu DVS, Majhi K, Kumar PSA, et al. Pressure-induced superconductivity in the weak topological insulator BiSe. *Phys Rev B* 2023;107:024506.
- [125] Li Q, Wu Y, Fan X, Zhang Y-J, Zhu X, Zhu Z, et al. Superconductivity arising from pressure-induced emergence of a Fermi surface in the Kagome lattice chalcogenide $\text{RB}_2\text{Pd}_3\text{Se}_4$. *Phys Rev B* 2022;106:214501.
- [126] Zhou Y et al. Pressure-induced metallization and robust superconductivity in pristine 1T-SnSe₂. *Adv Electron Mater* 2018;4:1800155.
- [127] Mu Q-G, Fan F-R, Borrmann H, Schnelle W, Sun Y, Felser C, et al. Pressure-induced superconductivity and modification of Fermi surface in type-II Weyl semimetal NbIrTe₄. *npj Quantum Mater* 2021;6:1–7.
- [128] Mozaffari S, Sun D, Minkov VS, Drozdov AP, Knyazev D, Betts JB, et al. Superconducting phase diagram of H₃S under high magnetic fields. *Nat Commun* 2019;10:2522.
- [129] Yue B, Zhong W, Deng W, Wen T, Wang Y, Yin Y, et al. Insulator-to-superconductor transition in quasi-one-dimensional HfS₃ under pressure. *J Am Chem Soc* 2023;145:1301–9.
- [130] Pei C, Zhang J, Wang Q, Zhao Y, Gao L, Gong C, et al. Pressure-induced superconductivity at 32 K in MoB₂. *Natl Sci Rev* 2023;10:nwad034.
- [131] Liu P, Peng F, Yin S, Liu F, Wang Q, Zhu X, et al. Exploring the behavior of molybdenum diboride (MoB₂): A high pressure x-ray diffraction study. *J Appl Phys* 2014;115:163502.
- [132] Okada H, Igawa K, Takahashi H, Kamihara Y, Hirano M, Hosono H, et al. Superconductivity under high pressure in LaFeAsO. *J Phys Soc Jpn* 2008;77:113712.
- [133] Wu W, Cheng J, Matsubayashi K, Kong P, Lin F, Jin C, et al. Superconductivity in the vicinity of antiferromagnetic order in CrAs. *Nat Commun* 2014;5:5508.
- [134] Yu Z, Wu W, Hu Q, Zhao J, Li C, Yang K, et al. Anomalous anisotropic compression behavior of superconducting CrAs under high pressure. *Proc Natl Acad Sci* 2015;112:14766–70.

- [135] Pei C, Xi M, Wang Q, Shi W, Wu J, Gao L, et al. Pressure-induced superconductivity in magnetic topological insulator candidate MnSb₄Te₇. *Phys Rev Mater* 2022;6:L101801.
- [136] Kurita N, Kimata M, Kodama K, Harada A, Tomita M, Suzuki HS, et al. Phase diagram of pressure-induced superconductivity in EuFe₂As₂ probed by high-pressure resistivity up to 3.2 GPa. *Phys Rev B* 2011;83:214513.
- [137] Yu Z, Wang L, Wang L, Liu H, Zhao J, Li C, et al. Conventional empirical law reverses in the phase transitions of 122-type iron-based superconductors. *Sci Rep* 2014;4:7172.
- [138] Torikachvili MS, Bud'ko SL, Ni N, Canfield PC. Pressure Induced Superconductivity in CaFe₂As₂. *Phys Rev Lett* 2008;101:057006.
- [139] Mittal R et al. Pressure dependence of phonon modes across the tetragonal to collapsed tetragonal phase transition in CaFe₂As₂. *Phys Rev B* 2010;81:144502.
- [140] Eguchi N, Kodama M, Ishikawa F, Nakayama A, Ohmura A, Yamada Y, et al. Powder x-ray diffraction of BaFe₂As₂ under hydrostatic pressure. *J Phys Conf Ser* 2012;400:022017.
- [141] Takahashi H et al. Pressure-induced superconductivity in the iron-based ladder material BaFe₂S₃. *Nat Mater* 2015;14:1008–12.
- [142] Hegger H, Petrovic C, Moshopoulou EG, Hundley MF, Sarrao JL, Fisk Z, et al. Pressure-induced superconductivity in quasi-2D CeRhIn₅. *Phys Rev Lett* 2000;84:4986–9.
- [143] Yamaoka H, Yamamoto Y, Schwier EF, Honda F, Zekko Y, Ohta Y, et al. Pressure and temperature dependence of the Ce valence and c-f hybridization gap in CeTIn₅ (T=Co, Rh, Ir) heavy-fermion superconductors. *Phys Rev B* 2015;92:235110.
- [144] Oomi G, Tabata M, Sakurai J. X-ray diffraction study of Ce(In_{1-x}Sn_xCe)₃ under high pressure. *J Magn Magn Mater* 1986;54–57:431–2.
- [145] Ohmura M, Sakai K, Nakano T, Miyagawa H, Oomi G, Sato I, et al. Anisotropic lattice compression and possible valence change in kondo compound CeAu₂Si₂. *J Magn Soc Jpn* 2009;33:31–4.
- [146] Ren Z, Pourovskii L, Giriat G, Lapertot G, Georges A, Jaccard D. Giant overlap between the magnetic and superconducting phases of CeAu₂Si₂ under pressure. *Phys Rev X* 2014;4:031055.
- [147] Li W, Feng J, Zhang X, Li C, Dong H, Deng W, et al. Metallization and superconductivity in the van der Waals compound CuP₂Se through pressure-tuning of the interlayer coupling. *J Am Chem Soc* 2021;143:20343–55.
- [148] Pei C, Zhang J, Gong C, Wang Q, Gao L, Zhao Y, et al. Distinct superconducting behaviors of pressurized WB₂ and ReB₂ with different local B layers. *Sci China Phys Mech Astron* 2022;65:287412.
- [149] Chi Z et al. Pressure-induced superconductivity in MoP. *npj Quantum Mater* 2018;3:1–7.
- [150] Li Y, An C, Hua C, Chen X, Zhou Y, Zhou Y, et al. Pressure-induced superconductivity in topological semimetal NbAs₂. *npj Quantum Mater* 2018;3:1–6.
- [151] Zhu J et al. Superconductivity in topological insulator Sb₂Te₃ induced by pressure. *Sci Rep* 2016;2013:3.
- [152] Yang H et al. Pressure-induced superconductivity in quasi-one-dimensional semimetal Ta₂PdSe₆. *Phys Rev Mater* 2022;6:084803.
- [153] Cai W, Lin W, Yan Y, Hilleke KP, Coles J, Bao J-K, et al. Pressure-induced superconductivity in the wide-band-gap semiconductor Cu₂Br₂Se₆ with a robust framework. *Chem Mater* 2020;32:6237–46.
- [154] Yuan Y, Wang W, Zhou Y, Chen X, Gu C, An C, et al. Pressure-induced superconductivity in topological semimetal candidate TaTe₄. *Adv Electron Mater* 2020;6:1901260.
- [155] Ganin AY, Takabayashi Y, Khimyak YZ, Margadonna S, Tamai A, Rosseinsky MJ, et al. Bulk superconductivity at 38 K in a molecular system. *Nat Mater* 2008;7:367–71.
- [156] Lim J, Hire AC, Quan Y, Kim J, Fanfarillo L, Xie SR, et al. High-pressure study of the low-Z rich superconductor Be₂₂Re. *Phys Rev B* 2021;104:064505.
- [157] Wang Q, Qiu X-L, Pei C, Gong B-C, Gao L, Zhao Y, et al. Superconductivity emerging from a pressurized van der Waals kagome material Pd₃P₂S₈. *New J Phys* 2023;25:043001.
- [158] Yu FH, Hua XY, Chen T, Sun J, Shi MZ, Zhuo WZ, et al. Pressure-induced superconductivity in a shandite compound Pd₃Pb₂Se₂ with the Kagome lattice. *New J Phys* 2020;22:123013.
- [159] Zhao Y, Hou J, Fu Y, Pei C, Sun J, Wang Q, et al. Pressure-induced superconductivity in PdTl with quasi-one-dimensional PdTe chains. *Crystals* 1833;2022:12.
- [160] Wang J, Chen X, Zhou Y, An C, Zhou Y, Gu C, et al. Pressure-induced superconductivity in trigonal layered PtBi₂ with triply degenerate point fermions. *Phys Rev B* 2021;103:014507.
- [161] Xu S, Zou Y, Sun J, Liu Z, Yu X, Gouchi J, et al. Physical properties and pressure-induced superconductivity in the single-crystalline band insulator SnO. *Phys Rev B* 2020;101:104501.
- [162] Shirotani I, Hayashi J, Adachi T, Sekine C, Kawakami T, Nakanishi T, et al. Metal to insulator transition of filled skutterudite PrRu₄P₁₂ at low temperatures and high pressures. *Phys B Condens Matter* 2002;322:408–12.
- [163] Miyake A, Shimizu K, Sekine C, Kihou K, Shirotani I. Pressure-induced superconductivity in filled skutterudite PrRu₄P₁₂. *J Phys Soc Jpn* 2004;73:2370–2.
- [164] Cao W, Zhao N, Pei C, Wang Q, Zhang Q, Ying T, et al. Pressure-induced superconductivity in the noncentrosymmetric Weyl semimetals LaAlX (X = Si, Ge). *Phys Rev B* 2022;105:174502.
- [165] Pan X-C, Chen X, Liu H, Feng Y, Wei Z, Zhou Y, et al. Pressure-driven dome-shaped superconductivity and electronic structural evolution in tungsten ditelluride. *Nat Commun* 2015;6:7805.
- [166] Yang H, Zhou Y, Wang S, Wang J, Chen X, Zhang L, et al. Pressure-induced nontrivial Z₂ band topology and superconductivity in the transition metal chalcogenide Ta₂Ni₃Te₅. *Phys Rev B* 2023;107:L020503.
- [167] Zhu C, Su H, Cheng E, Guo L, Pan B, Huang Y, et al. High-pressure study of topological semimetals XCd₂Sb₂ (X = Eu and Yb). *Chin Phys B* 2022;31:076201.